atmosphere

MDPI

Article

Quick Predictions of Onset Times and Rain Amounts from Monsoon Showers over Urban Built Environments

Siddharth Gumber [1] and Satyajit Ghosh [1,2,*]

[1] School of Mechanical Engineering, Vellore Institute of Technology, Vellore, Tamil Nadu 632014, India; siddharth.gumber@vit.ac.in
[2] School of Earth and Environment, University of Leeds, Leeds LS2 9JT, UK
* Correspondence: satyajitg@vit.ac.in

Abstract: Predicting the onset times of precipitation over densely populated cities for the purposes of timely evacuation is a challenge. This paper explored a flooding event over an urban built environment in a South Asian mega city, Chennai, where extant urban planning models rely on predicted rainwater amounts for early warning and impact assessment studies. However, the time duration of flooding events is related to the nature of the urban sprawl in the built environment. Any evacuation measure is invariably tied down to the time duration over which the precipitation event occurs, and therefore to the expected time of a precipitation event to begin. In this context, a crucial parameter useful to municipal authorities is the onset time of precipitation. This study used optimised analytical formulations to predict this time, and the derived analytical expressions for the case study yielded comparable times estimated from a computer-intensive full-scale large eddy model within an accuracy of 2%. It is suggested that municipal authorities (who are non-experts in fluid mechanics) use this early prediction for the purposes of quick alerts to a congested city's most vulnerable citizens within urban sprawls. However, for the procedure to work at its best, it involves a two-stage procedure. The first step involves the use of a parcel model to obtain the expected cloud droplet spectral spreads based on the prevailing dynamical characterisations. The second step involves an optimisation procedure involving cloud spectral properties from the first step to quantify both the auto-conversion rates and the threshold. Thereafter, an onset time calculation based on cloud properties is estimated. These new results are cast in closed form for easy incorporation into meteorological applications over a variety of urban scales. Rain mass amounts were also predicted analytically and used to configure Aeronautical Reconnaissance Coverage Geographic Information System (ARCGIS) to compute low drainage flow rates over the vulnerable parts of Chennai city. It was found that heavy precipitation over the North Chennai region yielded discharge rates to the tune of ~250 m^3s^{-1} during a 24 h period, causing intense flooding in the low-lying areas around the Cooum River basin with a large population density, with estimates sufficiently corroborating observations.

Keywords: planetary boundary layer; urban meteorology; auto-conversion; accretion; flooding alerts

Citation: Gumber, S.; Ghosh, S. Quick Predictions of Onset Times and Rain Amounts from Monsoon Showers over Urban Built Environments. *Atmosphere* **2022**, *13*, 370. https://doi.org/10.3390/atmos13030370

Academic Editor: Stefan Liess

Received: 3 January 2022
Accepted: 18 February 2022
Published: 23 February 2022

1. Introduction

Extreme rainfall events generally lead to urban flooding, and the commencement time of a heavy precipitation event is crucially important for the purposes of evacuation in densely populated parts of a city. City planners must ensure that evacuation routes are not blocked, and that the extent of flooding is predicted well in advance. The Intergovernmental Panel on Climate Change (IPCC) 6th assessment report asserts that when the global temperature threshold of 1.5 °C is exceeded, extreme precipitation events will severely impact large cities in subcontinental India including the cities of Kolkata, Chennai and Mumbai, which have millions of people housed in shanty towns [1]. Based on this grim forecast, it is important that a concrete plan is put in place so that quick-time alert

mechanisms are in place prior to a heavy precipitation event. Additionally, urban planning protocols must enforce regulations to control (if not altogether stop) unchecked flooding by relocating vulnerable citizens to safer areas, or through retrofitting of impervious surfaces. For instance, impermeable materials used for the building of paved surfaces and roads that affect rainfall run-off over evacuation routes can be unpaved. Satellite forecasts of cloud covers -[2] easily provide an indication of the spatial extent of cloudy regions over a city, and meteorological forecasts of extreme weather events, including a forecast of heavy precipitation, are also possible from observational and modelling studies. Models rely on the successful prediction of the onset times of precipitation for better flood management, and any evacuation measure is invariably tied down to the time duration over which the precipitation event occurs [3–5]. Earlier studies have highlighted that precipitation onset times as well as the initial storage levels in local water tanks are crucial parameters that modulate the extent of flooding in a region [6]. A sufficient lead time for planning and decision making is therefore crucial for mass evacuation efforts in vulnerable areas during heavy precipitation and cyclones [3].

A recent study by Pradhan et al. [7] discussed the relevance of predicting the onset times of precipitation events during the Indian Summer Monsoon period using modern state-of-the-art cloud models. However, quick predictions of onset times and precipitation amounts over localised regions as well as over vulnerable flood plains are still a challenge. Although Wilson et al. [8] stated that probabilistic predictions over large spatial extents are tractable, it is still worthwhile to explore deterministic predictions over smaller spatial extents through analytical calculations. Additionally, modellers face a challenge to include distinct aerosol signatures into cloud microphysical developments. Large-scale models use simple formulations to relate cloud droplet numbers to aerosol numbers. Sophisticated interpolation techniques are recommended for more accurate cloud droplet number counting (crucially important for rain amount quantification), particularly when polluted air masses with high aerosol loading contribute to cloud water amounts by drawing inferences from analogous droplet-driven airflows [9,10]. Newer studies are emerging to illustrate data assimilation techniques to better configure cloud microphysical schemes, particularly when both droplet sizes and numbers are used to compute cloud conversion. A recent paper by Vendrasco et al. [11] recommended the use of radar data assimilation for short-range local predictions using the widely used Weather Research and Forecasting (WRF) model configured with a double-moment microphysical scheme. At this stage, we wish to point out that the present paper used droplet spectral attributes within the remit of an optimised Kessler scheme for warm rain processes through the WRF double-moment scheme.

Current disaster mitigation policies are based on observational as well as empirical assessments of meteorological processes including severe precipitation events. Several South Asian cities are generally unprepared to face the brunt of such calamities. A seminal paper by Liu et al. [12] pointed out that models usually underestimate the expected severity of precipitation extremes because they ignore the intensification of such events over short time durations. These past studies suggest explorations into *all* pathways linked to precipitation events, and the present study therefore looks at not only the onset but also the aftermath. The prediction of onset times analytically for use in mobile telephony-based information dissemination must also be tested and benchmarked against a widely recognised CFD-based modelling analysis. If the onset times agree, only then can one justify the use of analytical results with computational overheads that cost only a fraction of a full-fledged cloud model. This benchmarking is achieved through the use of the widely recognised Weather Research and Forecasting (WRF) model [13].

In this paper, we illustrate the usefulness of analytical formulations for calculating the onset times of precipitation for warm clouds which occur frequently over tropical cities, including the southern Indian city of Chennai, home to 6 million people, which is our study area. With a judicious combination of auto-conversion rates and a threshold cloud water amount, it is possible to obtain a very quick estimate of the onset times of precipitation. The latter parameters are quantified by the widely used Kessler warm rain

scheme [14] (and subsequent adaptions: [15–20]) where the rates and the threshold are held fixed irrespective of the droplet spectral characteristics. This assumption is relaxed through a novel procedure where the threshold amount is first gauged from the developing cloud type. One expects that the process of auto-conversion of cloud water to rainwater is triggered when there are droplets with radii greater than 20 μm, meaning they have appreciable fall velocities to initiate the collection of droplets. New analytical formulations are presented to predict the time of commencement of precipitation by combining the processes of cloud auto-conversion and accretion, where collision–coalescence produces larger drops. The scheme of the paper is as follows:

1. A high-intensity precipitation event (1 December 2015) that caused catastrophic flooding over the southern Indian city is first described with a full meteorological discourse on the prevailing synoptic conditions (Figure 1).

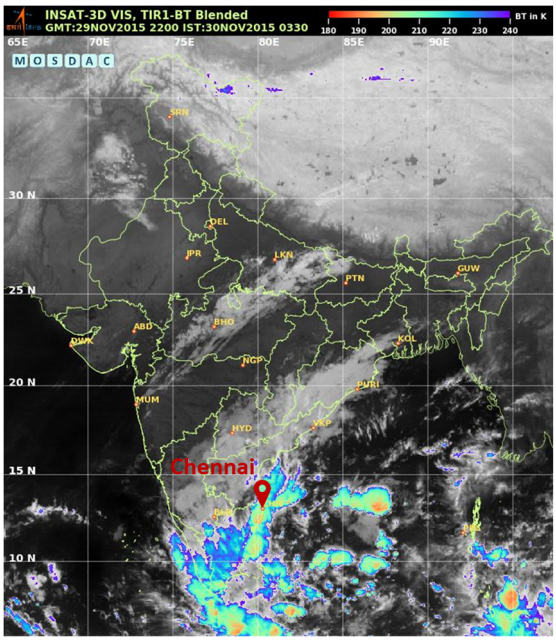

(**a**) (**b**)

Figure 1. (**a**) Submerged regions in Chennai during the heavy rainfall event in December 2015. Source: https://commons.wikimedia.org/wiki/File:Army_flood_relief_and_rescue_operations,_in_Chennai_on_November_17,_2015_(3).jpg (accessed on 15 December 2021). Licensed under CC BY-SA. (**b**) Cloud cover over the southern region of India on 1 December 2015 0130. Note the extensive cloud coverage over Chennai (13.0827° N, 80.2707° E).

2. The observed synoptic conditions and the associated cloud morphology are compared with results from a full-scale numerical weather prediction model which includes a double-moment microphysical scheme. Having obtained crucial information from a valuable CFD model run, the next step would be to estimate cloud spectral properties from a chemical parcel model ideally suitable for computing the growth of mixed aerosols over urban environments, resulting in the growth of both the smallest collected drops and the larger collector drops.
3. This is followed by a validation of the modelled cloud droplets with satellite-derived observations.
4. Analytical formulations are then derived to predict the onset time of precipitation combining the processes of cloud auto-conversion and accretion. This is a significant improvement over the standard Ghosh and Jonas [21] results, where the radii of the collected droplets (r) were completely ignored in the swept volume estimates. It

is shown that it is important to include these, and a much better agreement with observations is obtained when they are accounted for.

5. Modelled onset times are then predicted analytically from the rate of decrease in cloud water amounts. The e-folding time is a good indication of the expected onset time of precipitation of the event.
6. Finally, for the time duration over which the precipitation intensity was maintained at 15 mm/h, the associated discharge rates over the low-lying regions around the Cooum River basin with an urban sprawl of ~4 km^2 housing over 1 million residents are estimated.

2. Materials and Methods

2.1. Case study Description

The coastal cities of Tamil Nadu including Chennai and parts of Cuddalore experienced record levels of rainfall (∼490 mm on a single day) between 28 November and 2 December 2015, leading to ruinous flooding over the region [22,23]. The event caused 500 human casualties and a mass displacement to the tune of 1.8 million. Figure 1a shows a snapshot of submerged regions in Chennai city during this extreme precipitation event.

In what follows, we first describe the generic conditions for the synoptic development of a northeast monsoon cloud event (our case study) which was characterised by intense levels of precipitation, garnering media attention [22,24]. Figure 1b shows the cloud cover over peninsular India on 30 November 2015 0330 IST (Source: Meteorological & Oceanographic Satellite Data Archival Centre, Space Applications Centre, ISRO). The synoptic conditions during this period were characterised by north-westwardly moving low-pressure troughs which induced upper-level wind divergence and eventually deluged Chennai and other neighbouring regions—this was modelled with the Weather Research and Forecasting (WRF) model [13].

The WRF model (version: 3.8.1) was first run at a spatial resolution of 10 km × 10 km covering the city centre as well as all areas associated with urban sprawl and peripheral shanty towns. The real-time meteorological data (NCEP FNL data 1° × 1°) required for initialising the model were retrieved from the research data archive of the Computational and Information Systems Lab, National Centre for Atmospheric Research (NCAR). The simulation progressed from 29 November 2015 0000 h (0530 IST) to 06 December 2015 0000 h UTC (0530 IST) when distinct cloud activity was observed. The model set-up comprised 36 vertical levels up to 50 hPa and was subsequently integrated with a time step of 60 s. Cumulus convection was modelled through the widely used Kain–Fritsch scheme which is based on the mass flux approach for shallow and deep clouds [25]. The vertical structure of the boundary layer was resolved through Yonsei University's (YSU) planetary boundary layer (PBL) [26]. In addition, atmospheric heating from both incoming shortwave and outgoing longwave radiations was quantified using the Community Atmospheric Model (CAM) schemes [27,28]. In order to account for both the mass and the number concentration of the warm hydrometeors (cloud and rain droplets), a double-moment microphysical scheme (WDM6) was used. The cloud in question was predominantly warm (see Section 3); however, the microphysics option allowed the use of frozen hydrometeors as well.

The first step in this study was to ensure that, with the above specifications, we were able to get all the broad attributes right, so that one can proceed thereafter with further small-scale configurations. To this end, we first compared 2D distributions of the total precipitation with observations. For this reason, this preliminary comparison is briefly placed in this section.

Precipitation rates obtained from the model simulations (~15 mm/h over the central band) (Figure 2a) agreed favourably with the real-time TRMM precipitation data (URL: https://disc.gsfc.nasa.gov/datasets/TRMM_3B42_7/summaryTRMM2011, accessed on 15 December 2021) for 2 December 2015 between 1730 and 2030 IST over the chosen region (Figure 2b). Additionally, the model successfully captured the low-level wind

shear along the northeast direction. The modelled cloud base was positioned at 2.5 km (T~10 °C), with its top approaching an altitude of ~14 km over Chennai—a range very similar to LIDAR-based cloud depth observations (URL: https://www-calipso.larc.nasa.gov/products/, accessed on 15 December 2021). With these affirmations of cloud properties with observations, we proceeded further with a downscaled large eddy simulation to zoom in over the study region.

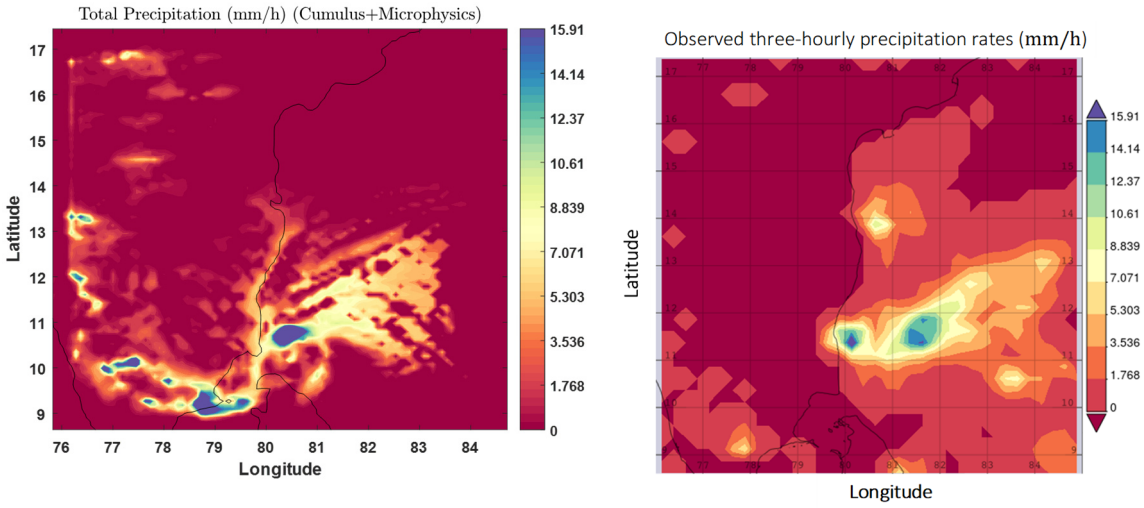

(**a**) (**b**)

Figure 2. Precipitation rates: (**a**) modelled total precipitation rate (mm/h) from WRF's WDM6 microphysical scheme; (**b**) observed three-hourly TRMM (Tropical Rainfall Measuring Mission) precipitation rates (mm/h) for 2 December 2015 12:00:00-15:00:00 (1730-2030 IST) (URL: https://disc.gsfc.nasa.gov/datasets/TRMM_3B42_7/summaryTRMM2011, accessed on 15 December 2021).

2.2. Large Eddy Simulation

Although the WRF with WDM6 was first executed over a coarse grid, it was necessary to undertake a finer-resolution run. In order to explicitly resolve the energy-containing eddies over the coastal metropolitan city of Chennai (13.0827° N, 80.2707° E), it was deemed appropriate to configure the WRF in the large eddy mode (LEM) in a manner outlined earlier by Bera and Prabha [29]. The spatial resolution was now held at 100 m × 100 m in the horizontal and 200 m in the vertical, covering a control volume with dimensions of 20 km× 20 km× 10 km. A much smaller time step of 1 s was required to capture essential details. Sub-grid-scale turbulence characterisation was conducted through a 1.5-order TKE closure scheme which used prognostic equations to characterise the eddy viscosity coefficients. The LEM was configured with weather soundings including vertical profiles of the potential temperature (θ), the relative humidity and components of the horizontal wind velocity vector (u and v winds) over Chennai for 1 December 2015 00:00:00 (0530 IST) (http://weather.uwyo.edu/upperair/sounding.html, accessed on 15 December 2021).

2.3. Parcel Model Simulation

Cloud spectral properties affect the partitioning of cloud water to rainwater. We assessed these properties with the use a sophisticated parcel model [30,31]. A Lagrangian chemical parcel model (CPM) was used that enables bin-wise growth of the dry aerosol particles into size-resolved cloud droplets [31–33]. The model was initialised with temperature, pressure, updraft speed and relative humidity values below the cloud base (see Table 1). From a perusal of the simulated vertical morphology of the cloudy region (see Section 3), a representative parcel updraft velocity of 1 ms^{-1} seemed appropriate (also see [34]) for the model simulation configured with the inputs listed in Table 1.

Table 1. Configuration of the chemical parcel model: key input variables.

Parameter	Cumulus Regime
Temperature	15 °C
Pressure at cloud base	823 hPa
Updraft speed at cloud base	1.0 ms^{-1}
Relative humidity at cloud base	91.0%
Parcel radius	500 m

3. Results

The high-resolution large eddy simulation (LES) yielded a detailed insight into the evolution of the cloud and rain amounts. Figure 3 shows time-varying cloud as well as liquid water paths (LWP) for the cloud in question.

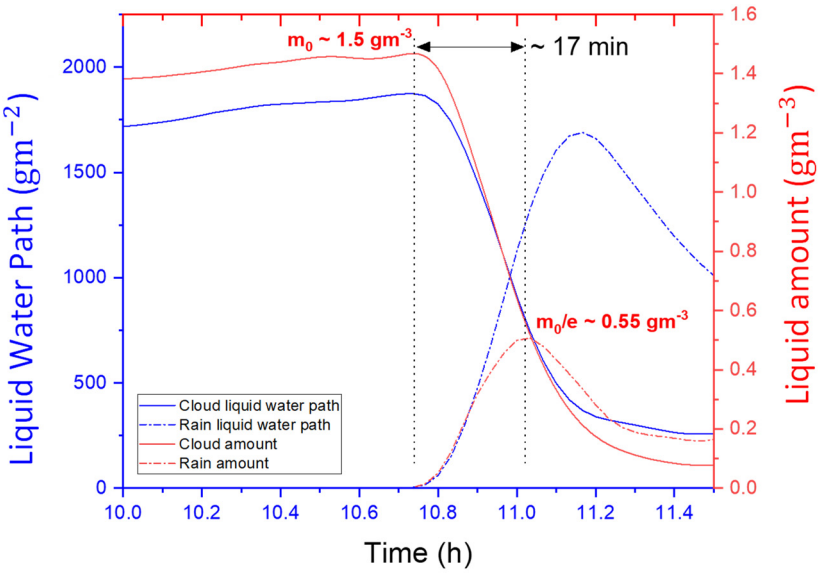

Figure 3. Temporal evolution of cloud and rainwater amounts and paths. Note that the rain mass increases with a sharp dip in cloud mass amounts, indicating efficient auto-conversion after 10.7 h (1608 IST). Note that the e-folding time was estimated to be 16.8 min.

The onset time of precipitation is generally a time measure for the initial cloud mass (m_0) to decrease to 1/e of the starting amount (Ghosh and Jonas [21]). One can notice from Figure 3 that the time taken for m_0 ~ 1.5 gm^{-3} to decrease to m_0/e ~ 0.55 gm^{-3} was indeed ~17 min.

It is observed in Figure 3 that the water mass was contained in the cloud as cloud water until 10.7 h, after which, owing to efficient auto-conversion and accretion, rain formation was triggered, with showers lasting for an hour. At this stage, it is also important to discuss the associated cloud morphology and the embedded temperature structure. Figure 4 makes a distinction between the warm and cold regions of the observed cloud, separated by a 0 °C isotherm (~4.5 km). A clear cloud base at 3 km is observed; however, small cloud patches are also noticed at lower levels between 2 and 3 km, in conformity with CALIPSO LIDAR observations for this day (URL: https://www-calipso.larc.nasa.gov/, accessed on 10 November 2021). The cloud-base temperature varied between 7.5 and 15 °C, confirming that the observed cloud was largely operated upon by warm rain microphysics. Observations also show a thick cloud band mainly composed of liquid water positioned between 2.5 and 5 km, in conformity with the modelled cloud morphology (Figure 4). Moreover, the modelled cloud droplet number density approached ~130 droplets cm^{-3}, in agreement with the MODIS (Moderate Resolution Imaging Spectroradiometer)-derived

cloud droplet number concentration of ~124 droplets cm^{-3} (dataset: MOD08_D3 v6.1 by Platnick et al. [35]; Grosvenor et al. [36]).

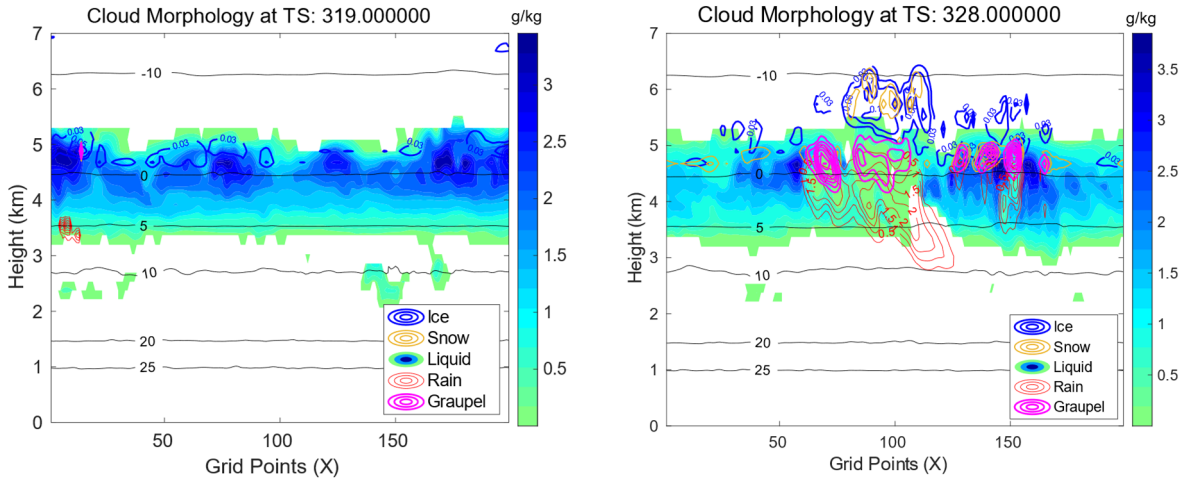

(**a**) (**b**)

Figure 4. Modelled cloud morphology over Chennai obtained from the LES model. (**a**) Hydrometeor distribution at ~10.7 h (1608 IST). (**b**) Cloud mixing ratios at 10.9 h (1626 IST). Note that turbulence and entrainment mediated indentations both at the cloud base and top. Horizontal contours (solid black lines) are isotherms in Celsius.

Figure 4a,b also illustrate the cloud conversion phase. During the initial period, cloud conversion into rain is observed at approximately 3.54 km above ground (red contours in Figure 4a; also see Figure 3). During the later stages, partitioning between the cloud and rain amounts was rapidly hastened over the upper reaches of the warm cloud (~4 km; see Figure 4b)—this was also observed in an earlier study [37].

Figure 5a,b clearly show cloud conversion into rain over vertical levels between 3 and 4 km (Figure 5a); subsequently, at a later stage (22 min beyond the initial time; see Figure 5b), one can observe that the rainwater mixing ratio rapidly increased—over these regimes, rain amounts increased contiguously as cloud amounts fell.

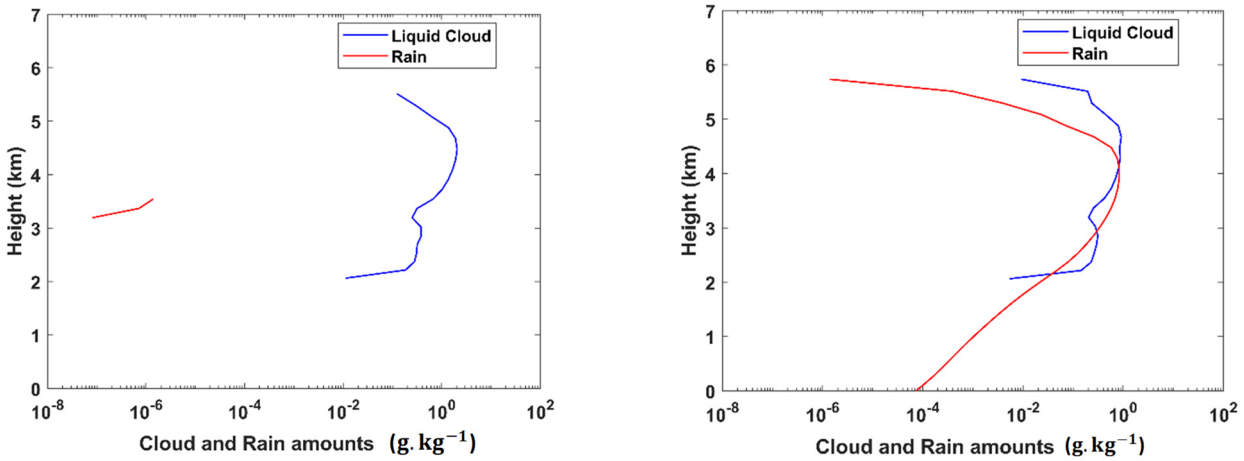

(**a**) (**b**)

Figure 5. Vertical profiles of cloud and rain mixing ratios at (**a**) the model time of ~10.7 h (1608 IST) and (**b**) 22 min past the initial time.

When we compare the modelled cloud morphology with the observations, we find that the case study in question pertained mainly to a warm case with liquid clouds subsuming an aerial coverage of ~63% (Figure 4)—a feature also corroborated by CALIPSO LIDAR observations, as stated earlier.

In the next section, we discuss how cloud spectral properties affected the partitioning of cloud water to rainwater. We assessed these properties with the use a sophisticated parcel model [30,31]. The processes of auto-conversion and accretion depend on how efficiently cloud droplets are able to group together to capture smaller cloud droplets, resulting in a spectral shift towards larger modes. Cloud conversion therefore depends on the spectral spread of droplets which, in turn, depends on the spreads of aerosol particle distributions—aerosols first activate into cloud condensation nuclei (CCN) to yield deliquesced droplets near the cloud base, a process captured by this sophisticated parcel model.

3.1. Cloud Droplet Spectral Growth

The dry aerosol profile (solid lines) over the city is shown in Figure 6, where the spectra comprise background sulphate (sourced from the oxidation of dimethyl sulfide (DMS) as well as from overland pollutants) and sea salt particles (film and jet modes sourced from the Bay of Bengal), along with partially soluble soot and black carbon particles mainly sourced from a heavy traffic flow in the city, termed the 'transient' mode [31,33,38,39]. From Figure 6, we find that the transient black carbon mode is sandwiched between the sulphate and the salt modes.

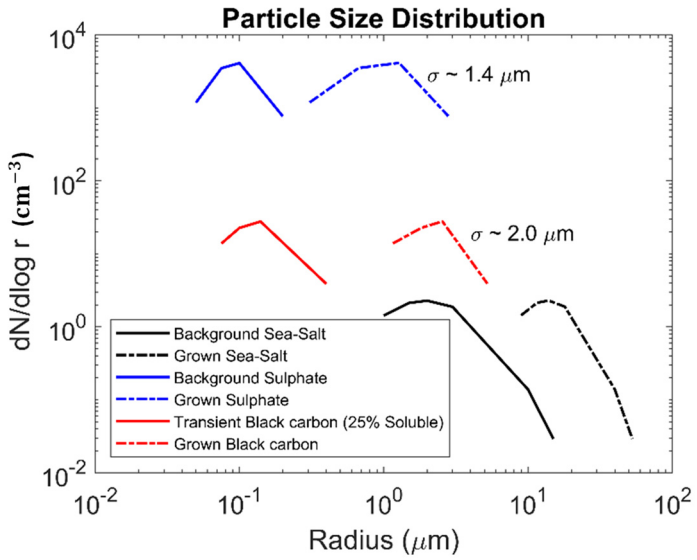

Figure 6. Resultant cloud droplet spectra near the cloud base grown from sulphate (fully soluble), black carbon (25% solubility) and natural sea salt aerosol (fully soluble). The spectra on the left (solid lines) pertain to dry aerosol size distributions; the background sulphate and sea salt modes were sourced from Gumber et al. (2020). The vehicle generated black carbon mode was derived experimentally (Kumar et al. 2019) and appropriately diluted. The spectra on the right are deliquesced droplets near the cloud base. The spectral width of each mode is also indicated.

The grown droplets near the cloud base are also shown (dashed lines) in Figure 6; one can immediately notice a shift to larger radii as compared to the starting dry aerosol radii for each mode.

The droplet spectral widths (σ) near the cloud base for the background sulphate and transient black carbon mode are 1.4 μm and 2.0 μm, respectively, in conformity with an earlier observational study [40]. Additionally, for the present study, an estimate of the mean volumetric radius, r_v, needed to be made. This was conducted based on the observed values of the effective radius, r_e (dataset: MOD08_D3 v6.1 by Platnick et al. [35];

Grosvenor et al. [36]). Assuming the 'k' parameter (a measure of the width of the modified gamma droplet distribution) value of 0.79 for convective clouds [36,41], since Chennai is a polluted city, we estimated r_v to be 17.5 μm, a number weighted average of all modes. We were then easily able to quantify the dispersion parameter near the cloud base ($D_b = \sigma/\bar{r}$) as 0.1. We show in the next section through new analytical formulations that cloud conversion times can be estimated by combining these spectral characteristics with an 'optimised' Kessler scheme.

3.2. Cloud Processes

3.2.1. Cloud Auto-conversion

Mass transfer of cloud water (m) into rainwater (M) is partly mediated by the process of auto-conversion, with a rate proportional to the cloud droplet fall velocity and the droplet cross-sectional area:

$$-\frac{dm}{dt} \propto V(r) \times \left(\pi r^2 N\right) \tag{1}$$

Here, m is the cloud mass $\left(g.m^{-3}\right)$, N is the cloud droplet number density (droplets m^{-3}) and $V(r)$ is the velocity of the falling cloud droplets. At this stage, it is important to discuss related research describing the process of auto-conversion. Kessler ([14]; his Equation (5)) initiated pioneering work, and the versatility and robustness of his work are testified by the fact that his procedures are still incorporated into many microphysical schemes in a variety of models including large eddy models, cloud-resolving models and the state-of-the-art WRF-ARW model [15–20,42]. Kessler chose to describe Equation (1) as

$$-\frac{dm}{dt} = k_1(m - a) \tag{2}$$

where he uses a constant, k_1 (s^{-1}), the auto-conversion rate, along with another constant, a (gm^{-3}), the auto-conversion threshold, with the caveat that auto-conversion is not allowed to proceed until cloud water amounts exceed this threshold. Assuming an r^2 dependence for the droplet fall velocity [43], the rate of depletion of cloud water can also be expressed as

$$-\frac{dm}{dt} = C_3 k_0 r^2 \times \left(\pi r^2 N\right) \tag{3}$$

where k_0 is 1.2×10^8 $m^{-1}s^{-1}$, and C_3 is a proportionality variable with units of liquid mass per unit volume of air. The bracketed quantity on the right-hand side is simply a measure of the total droplet cross-sectional area of a monodisperse droplet population with drop number density N (numbers/m^3). Since Equations (1) and (2) correspond to the same physical process, it is easy to show that

$$-\frac{dm}{dt} = k_1 m^{\frac{4}{3}} \tag{4}$$

where k_1, the auto-conversion rate, is given by $k_0 C_3 \pi N \left(\frac{3}{4\pi\rho N}\right)^{\frac{4}{3}}$. Equivalently, one can also express

$$-\frac{dm}{dt} = k_1 \times (m - a)^{\frac{4}{3}} \cong k_1(m - a) \tag{5}$$

One notices that, in the earliest formulation, Kessler approximated the 4/3 cloud water mass dependence to a linear mass dependence for simplifying the procedure. The Kessler formulation's easy incorporation into warm rain schemes stems from the fact that there are only two adjustable parameters that modellers use: the auto-conversion rate k_1, typically, ~10^{-3} s^{-1}, and the auto-conversion threshold (varies between 0.1 and 1 gm^{-3}). A

fuller expression without any approximation, but with the introduction of another rescaled constant for the auto-conversion, can be expressed as

$$-\frac{dm}{dt} = \frac{k_1}{C_3} \times m^{\frac{7}{3}} \cong k_1'' \times m^2 \quad (6)$$

Here, k_1'' is simply k_1/C_3. Equation (6) yields a quadratic cloud mass dependence for the rate of depletion of cloud water. However, the redeeming aspect of Equation (6) is that it naturally conforms to earlier power law parametrisations by Berry [42], Baker et al. [18] and Boucher et al. [19]. The quadratic dependence is compensated by the magnitude of the coefficient (k_1'') akin to a conversion rate but, in absolute terms, smaller than the original k_1 ($\sim 10^{-3}$ s^{-1}). The slowing down or speeding up of the auto-conversion process can be accounted for by varying values for the coefficient k_1'' in Equation (6) with a single constant. In contrast, Kessler [14] additionally invoked a second constant threshold a. Clearly, at first sight, Kessler, being linear, would be the preferred choice, but this choice comes with the cost of not accounting for droplet spectral properties. Ghosh and Jonas [21] described a procedure for optimising the standard Kessler with results from Berry's seminal paper (Berry [42]) to retain the overall simplicity of the Kessler formalism but were also able to include spectral properties of the droplets in their formalism. However, the Ghosh and Jonas [21] procedures were not applied to a full-scale cloud-resolving model (models such as the WRF were not developed at that time) and, importantly, ignored the small 'r' dependence altogether, i.e., the contribution of the settling of the collected drops with radius (r). These outstanding issues have been addressed in the present paper and are now discussed fully in Section 3.2.2.

Warm rain process optimisation procedures

We optimized the Kessler scheme with results from Berry [42], and the procedure proved to be extremely attractive because it could account for cloud spectral properties and any associated variations in the drop size distribution (DSD). Three cloud water conversion terms are now compared: the 'optimised' Kessler [14], the Berry [42] and the new correlation (present analyses; see Equation (6)). The 'optimisation' is visible in the solid blue line (Figure 7)—a realistic cloud auto-conversion threshold value of the order of 0.5 gm^{-3} was estimated based on a procedure from Yin et al. [44] for warm rain processes in Asian clouds. When cloud water amounts are less than this threshold, there is no change in the cloud water amounts; when exceeded, this results in a linear decline bound by the magnitude of the rate. The optimization, in essence, combines appropriate values of both the rate and the threshold to yield a decay curve, closely proxying the actual quadratic Berry curve (the continuously decreasing black and red curves in Figure 7). In fact, as we show later in the next section, the decay rates also yield a very realistic precipitation onset time.

3.2.2. Cloud Accretion

In this section, the process of accretion in the cloud conversion process is re-examined with the expectation that, even with the introduction of additional terms, the cloud conversion time can still be integrated analytically. For droplet accretion to proceed, the cloud in question must have some large collector drops (with radius $R > 20$ μm) as well as some collected smaller drops ($r < 20$ μm). Rain formation depends on both auto-conversion and accretion processes.

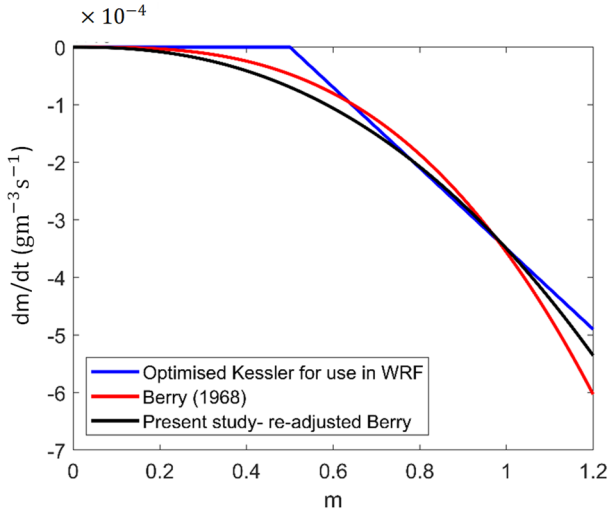

Figure 7. Optimising the Kessler scheme with the Berry scheme. Auto-conversion rate (k_1) and cloud threshold (a) obtained from the best fit of the standard Kessler (blue line plot) and Berry schemes (red line plot): $k_1 \sim 7\times10^{-4}$ s^{-1} and a = 0.5 gm^{-3}. Modified auto-conversion rate (k_1'') obtained from the best fit of the new auto-conversion correlation with the Berry schemes: $k_1'' = 3.5 \times 10^{-4}$ $\left(gm^{-3}\right)^{-1} s^{-1}$. Cloud parameters for this case study: N ~ 124 cm^{-3}, D_b ~ 0.1.

The rate of accreted rain mass (M) can be expressed as the volume swept out by the droplet of diameter D_i falling at a velocity V_i (Kessler [14]; his Equation (10)).

$$\frac{\delta M_i}{\delta t} = -\frac{\pi D_i^2}{4} E_i V_i m \tag{7}$$

Here, E_i is the collection efficiency with which the raindrop collects the falling cloud droplets of mass m. The rate of growth of the rain mass (M) in Equation (7) includes contributions from droplets of all sizes, and following Kessler, who invoked a Marshall–Palmer distribution to characterise the rain spectra, one is able to write

$$\frac{dM}{dt} = k_2' \times m M^{\frac{7}{8}} \cong k_2 \prime m M \tag{8}$$

Here, k_2' is $6.96 \times 10^{-4} E N_0^{\frac{1}{8}}$. In this study, we refrain from making the stringent assumption that Kessler originally made, i.e., the small collected drops have negligible cross-sectional areas and, consequently, fall velocities, and instead use the full collection equation as a starting point:

$$4\pi R^2 \frac{dR}{dt} = \frac{\pi}{\rho_l}(R+r)^2 \times |V(R) - V(r)| q_l \rho_a E(r,R) \tag{9}$$

For the case when the effect of small droplets is neglected ($r \to 0$ and $V(r) \sim 0$), one obtains

$$4\pi R^2 \frac{dR}{dt} = \frac{\pi}{\rho_l}(R)^2 \times |V(R)| q_l \rho_a E(r,R) \tag{10}$$

Equation (10) can be written as

$$4\pi \left(\frac{3M}{4\pi\rho N_R}\right)^{\frac{2}{3}} \frac{d}{dt}\left(\frac{3M}{4\pi\rho N_R}\right)^{\frac{1}{3}} = \frac{\pi}{\rho_l}\left(\frac{3M}{4\pi\rho N_R}\right)^{\frac{2}{3}} \times J \left(\frac{3M}{4\pi\rho N_R}\right)^{\frac{1}{3}} \times m \times E(r,R) \tag{11}$$

Here, $R = \left(\frac{3M}{4\pi\rho N_R}\right)^{\frac{1}{3}}$. After some algebra, we are able to retrieve the Kessler's original accretion and also the accretion term used by Ghosh and Jonas ([21]; their Equation (4)). This implies that

$$\frac{dM}{dt} \sim k_2 \prime mM \tag{12}$$

From Equation (9), however, one also obtains

$$-\frac{dm}{dt} = \frac{dM}{dt} = \pi N_R \left[AM^{\frac{1}{3}} + Bm^{\frac{1}{3}}\right]^2 \times \left|JAM^{\frac{1}{3}} - k_o B^2 m^{\frac{2}{3}}\right| mE \tag{13}$$

The fall velocity of the collector droplet in the collection equation is given by $V(R) = JR$ (for $R > 40$ μm), where $J = 8630\ s^{-1}$ [45]. Here, N_R is the rain drop number concentration, A and B are given by $\left(\frac{3}{4\pi\rho N_R}\right)^{\frac{1}{3}}$ and $\left(\frac{3}{4\pi\rho N}\right)^{\frac{1}{3}}$, respectively, and E ~ 0.1 in a cumulus cloud [46,47]. One can also notice that, significantly, the terms $\pi\left(Bm^{\frac{1}{3}}\right)^2$ and $k_o B^2 m^{\frac{2}{3}}$ represent, respectively, the cross-sectional area and the fall velocity of the small collector drops. We show in the next section that analytical solutions are still possible even after the inclusion of these additional terms.

3.2.3. Derivation of Precipitation Onset Times Analytically with Cloud Droplet Auto-Conversion and Accretion

The present study assumes a quadratic dependence on the cloud mass (m) in the auto-conversion term compared to a linear approximation on 'm' used in Ghosh and Jonas [21]. Additionally, the Ghosh and Jonas formalism completely ignored the small r dependence in the accretion term and assumed that the collector droplets accrete small cloud droplets with negligible cross-sectional areas and fall velocities. Closed-form analytical solutions are still obtained with new constants—a distinction is maintained between marine and continental cloud types as well based on the spectral distribution pattern. The cloud water depletion rates with the present new formulations can be written as

$$-\frac{dm}{dt} = \frac{dM}{dt} = k_1'' m^2 + \pi N_R \left[AM^{\frac{1}{3}} + Bm^{\frac{1}{3}}\right]^2 \times \left|JAM^{\frac{1}{3}} - k_o B^2 m^{\frac{2}{3}}\right| mE \tag{14}$$

Equation (14) is more representative of the combined effects of auto-conversion and accretion than the earlier Ghosh and Jonas ([21]; their Equation (4)):

$$-\frac{dm}{dt} = \frac{dM}{dt} = k_1(m - a) + k_2' mM^{\frac{7}{8}} \tag{15}$$

One notices that the new Equation (14) does not include an auto-conversion threshold, with this parameter often over-simplified by modellers due to a lack of observational data.

Equation (14) can be integrated to yield cloud conversion times:

$$t = -\int_{m_0}^{m} \frac{dm}{C'' m^3 + 2B'' m^2 + A'' m} \tag{16}$$

Here, $C'' = P/\left(3m_0^{\frac{2}{3}}\right) + Y/\left(3m_0^{\frac{1}{3}}\right)$, $2B'' = -\left(Pm_0^{\frac{1}{3}} + 2Z/3m_0^{\frac{1}{3}} + X - k_1'' + Ym_0^{\frac{2}{3}}\right)$, $X = \pi N_R A^3 JE$, $A'' = Xm_0 + Zm_0^{\frac{2}{3}}$, $Y = 2A^2B^2\pi N_R k_0 E$, $Z = 2A^2B\pi N_R JE$ and $P = 2AB^3\pi N_R k_0 E$. With the above simple formulation, one is simply required to judiciously prescribe numerical values of the constants A″, B″ and C″. These constants depend on microphysical parameters: (i) m_0, the initial cloud water amount; (ii) N, grown cloud droplet number concentration; (iii) N_R, rain droplet number concentration. By way of illustration, for the present case study corresponding to a heavy precipitation event over

a polluted urban city, the prescribed values are m_0 = 1.5 g/m^{-3} (see Figure 4), N = 124 droplets cm^{-3} and N_R = 5 droplets cm^{-3}, meaning that A″ = 0.0016, B″ = -3.175×10^{-4} and C″ = 2.8874×10^{-5}. Upon integration, two distinct cases emerge depending on the relative magnitudes of the constants A″, B″ and C″:

$$t = \frac{1}{A''}[\ln(m)]_{m_0}^{m} \quad B''^2 > A''C'' \\ -\frac{1}{2A''}\left[\ln\left(A'' + 2B''m + C''m^2\right)\right]_{m_0}^{m} - \frac{B''}{2A''\sqrt{B''^2 - A''C''}} \times \left[\ln\left(\frac{C''m + B'' - \sqrt{B''^2 - A''C''}}{C''m + B'' + \sqrt{B''^2 - A''C''}}\right)\right]_{m_0}^{m} \tag{17}$$

$$t = \frac{1}{A''}[\ln(m)]_{m_0}^{m} \quad B''^2 < A''C'' \\ -\frac{1}{2A''}\left[\ln\left(A'' + 2B''m + C''m^2\right)\right]_{m_0}^{m} - \frac{B''}{2A''\sqrt{B''^2 - A''C''}} \times \left[\tan^{-1}\left(\frac{C''m + B'' - \sqrt{B''^2 - A''C''}}{C''m + B'' + \sqrt{B''^2 - A''C''}}\right)\right]_{m_0}^{m} \tag{18}$$

For the present case study, with N $\sim$ 124 cm^{-3}, k_1'' $\sim 3.5 \times 10^{-4}$ $(gm^{-3})^{-1}s^{-1}$ and m_0 1.5 gm^{-3}, we observe that $B''^2 > A''C''$, meaning that Equation (17) should be used to compute the cloud water conversion rates. This is shown in Figure 8, where we show a comparison with the earlier Ghosh and Jonas [21] formulation which ignored the cross-sectional areas and fall velocities of the small collected cloud drops with radius r. The actual onset times are then estimated as an e-folding time, i.e., the time instance when the initial cloud water amount has depleted to 1/e of the original amount (m_0) is a measure of the onset time.

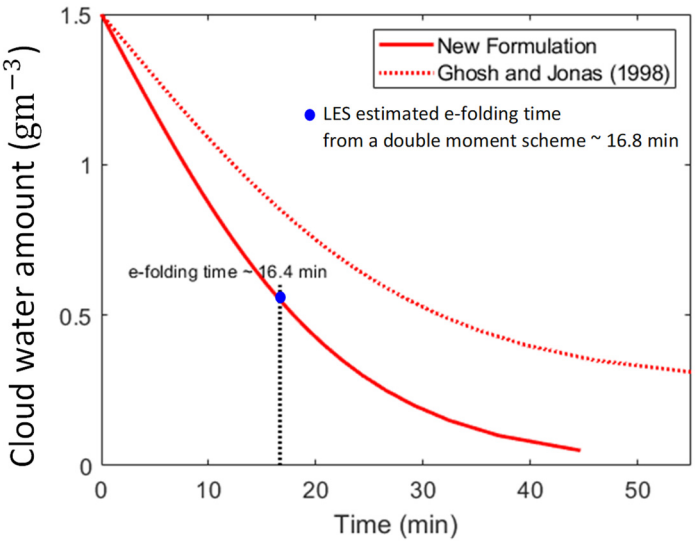

Figure 8. Onset time of precipitation estimated from analytical solutions (Equation (14a)) and the original Ghosh and Jonas (1998) calculations.

The obtained timescale (~16.4 min) for the initiation of precipitation from the new expressions compares well the WRF-LES simulation shown earlier (~16.8 min; see Figure 3), in contrast to an onset time of 26 min estimated from the Ghosh and Jonas [21] results. At this stage, it is important to compare the suitability of using Equations (17) and (18) for predicting the onset times of precipitation and to explore the possibility of precipitation alerts quickly without having to run a full-fledged large eddy simulation code. The latter requires a huge computational overhead on a LINUX platform typically run on a supercomputer, whereas the former can be coded in MATLAB, yielding the same forecast at a fraction of the cost when observational values of the input cloud water amount are known.

The preceding analyses showed that the onset time of precipitation estimated from analytical expressions closely matches the results from a full WRF simulation which included a double-moment microphysical scheme. The WRF also yielded intense precipitation rates

which city planners could use to better manage future city-scale flooding problems that are often acute over low-lying areas such as what was obtained over the North Chennai slums. To what extent did flooding overwhelm possible evacuation routes over the region? This question warrants a closer look, with the use of modelled precipitation amounts described earlier. Since the decrease in the cloud water mass, as shown in Figures 3 and 8, implies an increase in the rainwater mass ($-\mathrm{dm}/\mathrm{dt} = \mathrm{dM}/\mathrm{dt}$), the latter amounts (increasing with time) can also be easily plotted. The total integrated area under the rainwater production curve would then yield rain amounts as well. It must be noted, however, that, unlike in Equation (16) where the limits of time integration are $[m_0, m]$, one must bear in mind that rain does not proceed until after a time when m_0 reduces to m_0/e. The rain amounts estimated with this procedure (with the full formulation, where the collected drop cross-sectional areas and fall velocities are not neglected) numerically yield an amount of 0.55 gm^{-3}, as opposed to 0.25 gm^{-3} corresponding to a case when these are neglected. It is clear that the former amount agrees much more favourably with what is predicted from a full WRF-LES run (~ 0.6 gm^{-3}). In what we show next, we use the predicted rain intensities in ArcGIS to model drainage flow over North Chennai slums, a vulnerable area with a population of ~145,301 residing in an area spanning 4.28 km^2 [33,48] without access to appropriate drainage. To aggravate matters, the area in question is a low-lying area.

3.3. Rain Gauge Observations and Analytical Predictions of Rain Amounts

Rain gauges are deployed in significant numbers over peninsular India, enabling an in situ comparison of modelled rates with observations. Rainfall rates predicted from the new analytical solutions were compared with standard gauge estimates available from the Global Precipitation Mission's IMERG dataset centred around (13.0827° N, 80.2707° E) (GPM_3IMERGHH_V06; [49]). This gridded dataset (spatial resolution 0.1°) comprises precipitation estimates calibrated with real-time local rain gauge observations available over a selected region, in this instance, 'Chennai'. There are 14 operational rain gauge stations distributed across the city's geographical extent. Such deployments of gauge stations within the subcontinent generally follow the Bureau of Indian Standards norms (IS 5235:1992), which recommend the use of a 25 mm rain gauge capable of recording even intense precipitation events—the current case study also pertains to such an event. Assuming the spatial homogeneity of the received precipitation, 1 mm of accumulated rainwater in the measuring cylinder is equivalent to a litre of rainwater collected over a unit square metre. To estimate the rainfall rates from the formulations shown in Equation (14), one must simply compute the associated precipitation fluxes by integrating the rainwater production rates (dM/dt) ($\mathrm{kgm}^{-3}\mathrm{s}^{-1}$) over cloud levels with rain within the cloud deck (also see Figure 8). Two distinct model time slots corresponded to gauge collection times ranging between 11:32:00 UTC (1702 IST) and 11:55:00 UTC (1725 IST) on 1 December 2015. The precipitation fluxes were estimated to be 7.69 $\times 10^{-4}$ $\mathrm{kgm}^{-2}\mathrm{s}^{-1}$ and 1.24 $\times 10^{-3}$ $\mathrm{kgm}^{-2}\mathrm{s}^{-1}$, respectively, yielding rain amounts of 2.7 mm/h and 4.47 mm/h, comparing reasonably well with the observed values of 3 mm/h and 4.9 mm/h. These results are summarised in Table 2.

Table 2. Rain Gauge observations and Analytical Predictions of Rain Amounts.

Time Instance	Rain Rates from Analytical Solutions (mm/h)	Observed Rain Rates (mm/h)	% Error
11:32:00 UTC	2.70	3	10
11:55:00 UTC	4.47	4.9	8.7

An additional dataset was also available around mid-day for this date at Nungambakkam (13.05°N, 80.24°E) located within the city centre and close to the earlier Integrated Multi-satellitE Retrievals for GPM (IMERG) domain. A value of 5 mm/h was reported by Phadtare et al. [50], which also compares well with the modelled value of 4.47 mm/h.

3.4. Modelling Drainage Flow over Inundated North Chennai Slums

Chennai city received nearly 300% above normal rainfall during late November and early December in 2015. The extreme precipitation event caused incessant flooding in several low-lying regions because of an improper drainage system [51]. These areas include Madhavaram, Tondiarpet, Tiruvottiyur, Manali and Royapuram (see Figure 9) and account for nearly 34% of the total slum population in the city [33]. The total geographic area and slum population for each region are, respectively, (7.2×10^5 m^2, 21,968), (1.6×10^6 m^2, 35,644), (7.1×10^5 m^2, 33,702), (5.1×10^5 m^2, 22,405) and (7.4×10^5 m^2, 31,582).

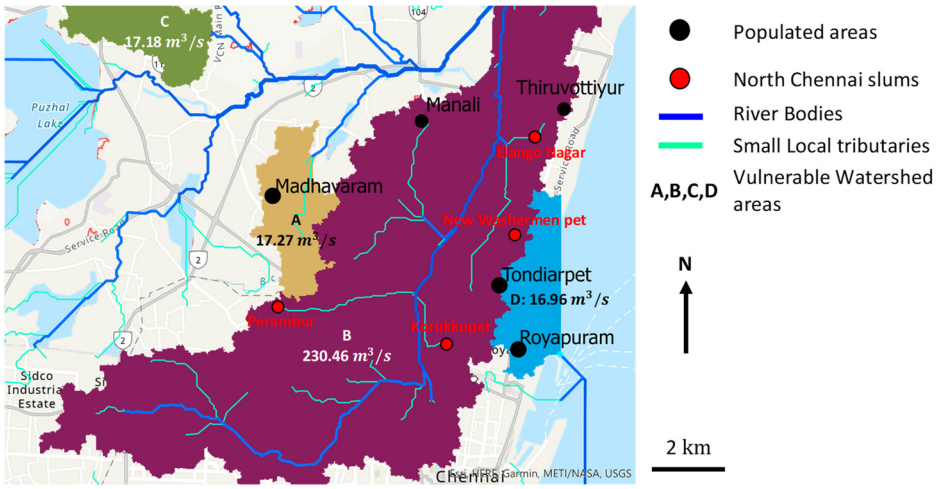

Figure 9. Drainage map of the study region generated from GIS showing major river streams, tanks and vulnerable watershed areas in the North Chennai slum region (Madhavaram, Manali, Thiruvottiyur, Tondiarpet and Royapuram). Region-wise run-off rates are indicated in each watershed area (see number indicated below regions marked A, B, C and D).

The areas in question, north Thiruvottiyur covering Kathivakkam, the Ennore region, west Madhavaram and the Surappattu area near Puzhal Lake, were developed over the reclaimed Kosasthalai wetland (see Figure 9). This is a natural system classed under herbaceous wetlands (USGS land-use category 17; [52]). Such wetlands generally act as buffers and soak up surplus flow of water. Recent urbanisation has led to changes in the city's land use patterns. Whilst development projects over the city's prime districts were heavily concreted, contributing to the urban heat island effect, the parts over the study areas were mainly shanty towns built with cheap materials which include thatch, corrugated sheets, mud walls, plastic and bricks. Even with the inclusion of such makeshift constructed areas adjoining the lake regions, the ratio of the built-up land to natural land mass is still low at around 0.20 (Kathivakkam) and 0.30 (Madhavaram) in comparison to the city's high overall built-up ratio of 0.53 (http://www.cmdachennai.gov.in/, accessed on 10 November 2021). Heavily urbanised cities in developed countries have, of course, significantly higher ratios (the City of London: 0.98; [53]). This low built-up ratio around natural riverine systems partly justifies the use of DEM in ArcGIS, as also attested by Hamdy et al. [54].

It is thus imperative to delineate drainage patterns as well as spill regions in the city's most vulnerable zones; this was achieved through a sophisticated disaster mitigation model, ArcGIS, which was run with inputs of precipitation amounts obtained from procedures outlined in the previous section.

ArcGIS is a geographical information system model which facilitates the handling and analyses of geographical information through image digitisation procedures [55]. Watershed delineation in ArcGIS is a six-step procedure involving, first, the usage of the Fill tool applied to a DEM file. This step quality checks the elevation file and removes surface imperfections (the DEM file for the present case study was sourced from Bhuvan,

which is a geo-platform managed by the Indian Space Research Organisation (ISRO); URL: https://bhuvan.nrsc.gov.in/home/index.php, accessed on 10 November 2021). This is followed by ascertaining the flow directions using the Flow Direction algorithm which determines the flow of water across the surface based on the topography of the landscape. Subsequently, the Flow Accumulation tool is used to identify the upstream cells flowing into the downstream grids. In essence, the low-lying areas subsume cells with higher flow accumulation values. To demarcate the watersheds, pour points are identified near the exposed regions through a handle on the flow direction raster. The pour points are subsequently snapped to the closest cell of a high flow accumulation before using the Watershed algorithm. Figure 9 shows the drainage map of the study region generated from GIS showing major river streams and tanks along with the vulnerable watersheds in the North Chennai slum region. The heavily populated areas as well as the slum regions are shown with black and red markers, respectively.

From Figure 9, the shanty town settlements fall within a major watershed region with an overall spill area of 230 km^2. Town planners should be able to cope with very intense precipitation events, particularly because shanty towns house impoverished and vulnerable citizens who live in makeshift dwellings. Although the analytical formulations pertained to a case study where the city was flooded, the precipitation intensity of 15 mm/h was not a one-off event—17 mm/h was also recorded for the NE monsoon season over this city in 2005 (TRMM TRMM_3B42 v7; [56]). For these reasons, the expected flooding rates over the study regions covering the pour points located near New Washermenpet, Royapuram, Madhavaram and Puzhal Lake (see Figure 9) were assessed for a value of 15 mm/h observed during 2015. The rates of water discharge into regions A, B, C and D were 17.27 m^3/s, 230.46 m^3/s, 17.18 m^3/s and 16.96 m^3/s, respectively, for a chosen run-off coefficient value of 0.70 (Subramanya [57]) for built-up areas. The estimated values are in conformity with the flood discharge rates calculated in urban areas by Konrad [58]. One can also estimate the height of water accumulated through a handle on the volumetric discharge rates. For instance, for region A (Madhavaram), the flooding depth during a 24 h period was estimated to be ~0.3 m, in agreement with the flood depth calculation published in the Red Atlas developed by the National Centre for Coastal Research (NCCR) for the selected region (URL: https://timesofindia.indiatimes.com/city/chennai/30cm-of-rainfall-in-a-day-could-flood-most-parts-ofchennai/articleshow/72728786.cms, accessed on 15 December 2021). The methodology described in Section 3 provides a holistic timescale and region-specific guidelines to retard (if not altogether stop) extended flooding by altering vulnerable parts.

4. Conclusions

This paper yielded new analytical formulations to compute onset times of precipitation and the conversion of cloud water to rainwater, yielding mass rain amounts. The predicted onset times and the mass rain amounts agree very well with the times and amounts obtained from a full WRF model run using the double-moment scheme. Since rain gauges are deployed in significant numbers over peninsular India, it was necessary to compare the precipitation intensities in mm/h from standard gauge observations. It was found that the analytically predicted rain amounts compared favourably with rain gauge observations for the chosen date, i.e., 1 December 2015 11:32:00 (1702 IST) to 11:55:00 UTC (1725 IST). It must be pointed out that the analytical formulations work best for warm rain parts of the cloud. Owing to their analytical closed-form nature, one has three distinct advantages: (i) A quick prediction of the approximate onset times of precipitation can be obtained from satellite observational procedures outlined by Li et al. [59] and Rosenfeld et al. [60]. This foreknowledge will help in planning and preparedness strategies. (ii) The modelled precipitation amounts can be used within ArcGIS to yield almost instantaneous locations of spill areas so that vulnerable parts are quickly identified (Hamdy et al., 2016). (iii) The ArcGIS outputs combining information from (i) and (ii) can then be used in a separate protocol coded in MATLAB to yield the drainage flow rates, again instantaneously, over

the identified spill areas from run-off coefficient estimates given by Subramanya [57] and Konrad [58]. For example, following procedures (i–iii), it was found that precipitation set in within a time span of ~17 min, yielding strong drainage flow over the North Chennai slums housing a huge population over a limited spatial extent of only about 4 km^2.

The widely used Weather Research and Forecasting model run in the double-moment mode was used to compare the analytically predicted onset times and rain amounts, where very good agreement was found (analytical and modelled estimates of onset time of precipitation were, respectively, 16.4 min and 16.8 min, whilst the rain amounts were 0.55 gm^{-3} and 0.6 gm^{-3}, respectively). It is suggested that these formulations be used to obtain expected onset times of precipitation from satellite as well as radar-based observations not only for alerting operations but also for new impact assessment studies prior to any development activities that might trigger flooding.

Author Contributions: S.G. (Siddharth Gumber) and S.G. (Satyajit Ghosh) contributed to the study conception and design. S.G. (Siddharth Gumber) performed all the model simulations and related analytical derivations. Both authors interpreted the results. All authors have read and agreed to the published version of the manuscript.

Funding: This article received no funding.

Institutional Review Board Statement: Not applicable.

Informed Consent Statement: Not applicable.

Data Availability Statement: Not applicable.

Acknowledgments: The authors sincerely thank the School of Mechanical Engineering (SMEC), VIT Vellore and the Centre for Technical Support (CTS) for providing computing resources under the Erasmus+ Scheme 'Capacity Building in the field of Higher Education 2019 (CBHE2019)'.

Conflicts of Interest: The authors declare no conflict of interest.

References

1. Masson-Delmotte, V.; Zhai, P.; Pirani, A.; Connors, S.L.; Péan, C.; Chen, Y.; Goldfarb, L.; Gomis, M.I.; Matthews, J.B.R.; Berger, S.; et al. (Eds.) *Climate Change 2021: The Physical Science Basis. Contribution of Working Group I to the Sixth Assessment Report of the Intergovernmental Panel on Climate Change*; Cambridge University Press: Cambridge, UK, 2021.
2. Saini, I.; Chandramouli, P.; Samaddar, A.; Ghosh, S. Quantifying Tropical Cyclone Cloud Cover Using Envisat Retrievals—An Example of a Recent Severe Tropical Cyclone, 'Thane'. *Int. J. Remote Sens.* **2013**, *34*, 4933–4950. [CrossRef]
3. Ghosh, S.; Vidyasagaran, V.; Sandeep, S. Smart cyclone alerts over the Indian subcontinent. *Atmos. Sci. Lett.* **2013**, *15*, 157–158. [CrossRef]
4. Ghosh, S.; Sharma, A.; Arora, S.; DeSouza, G. A geoengineering approach toward tackling tropical cyclones over the Bay of Bengal. *Atmos. Sci. Lett.* **2016**, *17*, 208–215. [CrossRef]
5. Lee, Y.H.; Kim, H.I.; Han, K.Y.; Hong, W.H. Flood Evacuation Routes Based on Spatiotemporal Inundation Risk Assessment. *Water* **2020**, *12*, 2271. [CrossRef]
6. Devi, N.N.; Sridharan, B.; Bindhu, V.M.; Narasimhan, B.; Bhallamudi, S.M.; Bhatt, C.M.; Usha, T.; Vasan, D.T.; Kuiry, S.N. Investigation of Role of Retention Storage in Tanks (Small Water Bodies) on Future Urban Flooding: A Case Study of Chennai City, India. *Water* **2020**, *12*, 2875. [CrossRef]
7. Pradhan, M.; Rao, A.S.; Srivastava, A.; Dakate, A.; Salunke, K.; Shameera, K.S. Prediction of Indian Summer-Monsoon Onset Variability: A Season in Advance. *Sci. Rep.* **2017**, *7*, 14229. [CrossRef] [PubMed]
8. Wilson, J.W.; Feng, Y.; Chen, M.; Roberts, R.D. Nowcasting Challenges during the Beijing Olympics: Successes, Failures, and Implications for Future Nowcasting Systems. *Weather Forecast.* **2010**, *25*, 1691–1714. [CrossRef]
9. Rap, A.; Ghosh, S.; Smith, M.H. Shepard and Hardy Multiquadric Interpolation Methods for Multicomponent Aerosol–Cloud Parameterization. *J. Atmos. Sci.* **2009**, *66*, 105–115. [CrossRef]
10. Ghosh, S.; Phillips, J.C.; Perkins, R.J. Modelling the Flow in Droplet-Driven Sprays. In *Advances in Turbulence 3*; Johansson, A.V., Alfredsson, P.H., Eds.; Springer: Berlin/Heidelberg, Germany, 1991. [CrossRef]
11. Vendrasco, E.P.; Machado, L.A.T.; Ribeiro, B.Z.; Freitas, E.D.; Ferreira, R.C.; Negri, R.G. Cloud-Resolving Model Applied to Nowcasting: An Evaluation of Radar Data Assimilation and Microphysics Parameterization. *Weather Forecast.* **2020**, *35*, 2345–2365. [CrossRef]
12. Liu, S.C.; Fu, C.; Shiu, C.-J.; Chen, J.-P.; Wu, F. Temperature Dependence of Global Precipitation Extremes. *Geophys. Res. Lett.* **2009**, *36*. [CrossRef]

13. Skamarock, W.C.; Klemp, J.; Dudhia, J.; Gill, D.O.; Barker, D.; Wang, W.; Powers, J.P. *A Description of the Advanced Research WRF Version 3*; University Corporation for Atmospheric Research: Boulder, CO, USA, 2008; Volume 27, pp. 3–27.
14. Kessler, E. *On the Distribution and Continuity of Water Substance in Atmospheric Circulations*; American Meteorological Society: Boston, MA, USA, 1969.
15. Manton, M.J.; Cotton, W.R. *Formulation of Approximate Equations for Modeling Moist Deep Convection on the Mesoscale*; Atmospheric Science Paper 266; Colorado State University: Fort Collins, CO, USA, 1977; 62p.
16. Tripoli, G.J.; Cotton, W.R. A numerical investigation of several factors contributing to the observed variable intensity of deep convection over South Florida. *J. Appl. Meteor.* **1980**, *19*, 1037–1063. [CrossRef]
17. Liou, K.N.; Ou, S.C. The role of cloud microphysical processes in climate: An assessment from a one-dimensional perspective. *J. Geophys. Res.* **1989**, *94D*, 8599–8607. [CrossRef]
18. Baker, M.B. Variability in concentrations of cloud condensation nuclei in the marine cloud-topped boundary layer. *Tellus B Chem. Phys. Meteorol.* **1993**, *45*, 458–472. [CrossRef]
19. Boucher, O.; Treut, H.L.; Baker, M.B. Precipitation and radiation modeling in a general circulation model: Introduction of cloud microphysical process. *J. Geophys. Res.* **1995**, *100D*, 6395–16414. [CrossRef]
20. Noh, Y.; Oh, D.; Hoffmann, F.; Raasch, S. A Cloud Microphysics Parameterization for Shallow Cumulus Clouds Based on Lagrangian Cloud Model Simulations. *J. Atmos. Sci.* **2018**, *75*, 4031–4047. [CrossRef]
21. Ghosh, S.; Jonas, P.R. On the application of the classic Kessler and Berry schemes in Large Eddy Simulation models with a particular emphasis on cloud autoconversion, the onset time of precipitation and droplet evaporation. *Ann. Geophys.* **1998**, *16*, 628–637. [CrossRef]
22. Jayaraman, N. Why Is India's Chennai flooded? *BBC News*. Available online: https://www.bbc.com/news/world-asia-india-34992004 (accessed on 19 February 2022).
23. IMD (Indian Meteorological Department). Heavy Rainfall over Southeast India during November 2015: A Report. 2015. Available online: https://nwp.imd.gov.in/NWP-CHENNAI-RAINFALL-REPORT-2015.pdf (accessed on 19 February 2022).
24. Biswas. Remembering 2015 Chennai Flood: How the City Suffered and Survived Heavy Rains 2 Years Back. In India Today. 2017. Available online: https://www.indiatoday.in/fyi/story/chennai-heavy-rains-news-2015-flood-december-1075731-2017-11-04 (accessed on 8 July 2021).
25. Kain, J.S. The Kain–Fritsch Convective Parameterization: An Update. *J. Appl. Meteorol. Climatol.* **2004**, *43*, 170–181. [CrossRef]
26. Hong, S.-Y.; Noh, Y.; Dudhia, J. A New Vertical Diffusion Package with an Explicit Treatment of Entrainment Processes. *Mon. Weather Rev.* **2006**, *134*, 2318–2341. [CrossRef]
27. Ramanathan, V.; Downey, P. A nonisothermal emissivity and absorptivity formulation for water vapor. *J. Geophys. Res. Earth Surf.* **1986**, *91*, 8649–8666. [CrossRef]
28. Briegleb, B.P. Delta-Eddington approximation for solar radiation in the NCAR community climate model. *J. Geophys. Res. Earth Surf.* **1992**, *97*, 7603. [CrossRef]
29. Bera, S.; Prabha, T.V. Parameterization of Entrainment Rate and Mass Flux in Continental Cumulus Clouds: Inference from Large Eddy Simulation. *J. Geophys. Res. Atmos.* **2019**, *124*, 13127–13139. [CrossRef]
30. O'Dowd, C.D.; Lowe, J.A.; Smith, M.H. Coupling sea-salt and sulphate interactions and its impact on predicting cloud droplet concentrations. *Geophys. Res. Lett.* **1999**, *26*, 1311–1314. [CrossRef]
31. Ghosh, S.; Smith, M.; Rap, A. Integrating biomass, sulphate and sea-salt aerosol responses into a microphysical chemical parcel model: Implications for climate studies. *Philos. Trans. R. Soc. London. Ser. A Math. Phys. Eng. Sci.* **2007**, *365*, 2659–2674. [CrossRef] [PubMed]
32. Ghosh, S.; Gumber, S.; Varotsos, C. A Sensitivity Study of Diffusional Mass Transfer of Gases in Tropical Storm Hydrometeors. *Theor. Appl. Climatol.* **2018**, *134*, 1083–1100. [CrossRef]
33. Gumber, S.; Ghosh, S.; Orr, A.; Sathish Kumar, C.R.; Pope, J. On the Microphysical Processing of Aged Combustion Aerosols Impacting Warm Rain Microphysics over Asian Megacities. *Theor. Appl. Climatol.* **2020**, *139*, 1479–1491. [CrossRef]
34. Ghosh, S.; Osborne, S.; Smith, M.H. On the importance of cumulus penetration on the microphysical and optical properties of stratocumulus clouds. *Atmos. Chem. Phys.* **2005**, *5*, 755–765. [CrossRef]
35. Platnick, S.; Hubanks, P.; Meyer, K.; King, M.D. MODIS Atmosphere L3 Monthly Product (08_L3). NASA MODIS Adaptive Processing System, Goddard Space Flight Center. 2015. Available online: https://doi.org/10.5067/MODIS/MOD08_M3.006 (accessed on 19 February 2022).
36. Grosvenor, D.P.; Sourdeval, O.; Zuidema, P.; Ackerman, A.; Alexandrov, M.D.; Bennartz, R.; Boers, R.; Cairns, B.; Chiu, J.C.; Christensen, M.; et al. Remote Sensing of Droplet Number Concentration in Warm Clouds: A Review of the Current State of Knowledge and Perspectives. *Rev. Geophys.* **2018**, *56*, 409–453. [CrossRef]
37. Hoffmann, F.; Noh, Y.; Raasch, S. The Route to Raindrop Formation in a Shallow Cumulus Cloud Simulated by a Lagrangian Cloud Model. *J. Atmos. Sci.* **2017**, *74*, 2125–2142. [CrossRef]
38. Safai, P.D.; Raju, M.P.; Maheshkumar, R.S.; Kulkarni, J.R.; Rao, P.S.P.; Devara, P.C.S. Vertical Profiles of Black Carbon Aerosols over the Urban Locations in South India. *Sci. Total Environ.* **2012**, *431*, 323–331. [CrossRef] [PubMed]
39. Kumar, C.R.S.; Gumber, S.; Gumber, S.; Mishra, R.; Jeyaseelan, T.; Yang, H. Carbonaceous Particle Scavenging and Thermal Comfort Augmentation with an Extended Green Facade Draped with Vernonia elaeagnifolia. *EnvironmentAsia* **2019**, *12*, 6274. [CrossRef]

40. Prabha, T.V.; Patade, S.; Pandithurai, G.; Khain, A.; Axisa, D.; Pradeep-Kumar, P.; Maheshkumar, R.S.; Kulkarni, J.R.; Goswami, B.N. Spectral width of premonsoon and monsoon clouds over Indo-Gangetic valley. *J. Geophys. Res. Earth Surf.* **2012**, *117*. [CrossRef]
41. Martin, G.M.; Johnson, D.W.; Spice, A. The Measurement and Parameterization of Effective Radius of Droplets in Warm Stratocumulus Clouds. *J. Atmos. Sci.* **1994**, *51*, 1823–1842. [CrossRef]
42. Berry, E.X. Modification of the warm rain process. In Proceedings of the First Conference on Weather Modification; AMS: Albany, NY, USA, 1968; pp. 81–88.
43. Ghosh, S.; Jonas, P.R. Some analytical calculations on the effect of turbulence on the settling and growth of cloud droplets. *Geophys. Res. Lett.* **2001**, *28*, 3883–3886. [CrossRef]
44. Yin, J.; Wang, D.; Zhai, G. An attempt to improve Kessler-type parameterization of warm cloud microphysical conversion processes using CloudSat observations. *J. Meteorol. Res.* **2015**, *29*, 82–92. [CrossRef]
45. Johnson, D. The role of giant and ultragiant aerosol particles in warm rain initiation. *J. Atmos. Sci.* **1982**, *39*, 448–460. [CrossRef]
46. Jonas, P. Turbulence and cloud microphysics. *Atmos. Res.* **1996**, *40*, 283–306. [CrossRef]
47. Chen, S.; Yau, M.K.; Bartello, P. Turbulence Effects of Collision Efficiency and Broadening of Droplet Size Distribution in Cumulus Clouds. *J. Atmos. Sci.* **2018**, *75*, 203–217. [CrossRef]
48. Chandramouli, C. Slums in Chennai: A Profile. In Proceedings of the Third International Conference on Environment and Health, Chennai, India, 15–17 December 2003; Bunch, M.J., Suresh, M.V., Kumaran, T.V., Eds.; Department of Geography, University of Madras and Faculty of Environmental Studies, York University: Chennai, India, 2003; pp. 82–88.
49. Huffman, G.J.; Stocker, E.F.; Bolvin, D.T.; Nelkin, E.J.; Tan, J. GPM IMERG Final Precipitation L3 Half Hourly 0.1 Degree × 0.1 Degree V06, Greenbelt, MD, Goddard Earth Sciences Data and Information Services Center (GES DISC). Available online: 10.5067/GPM/IMERG/3B-HH/06 (accessed on 25 January 2022).
50. Phadtare, J. Role of Eastern Ghats Orography and Cold Pool in an Extreme Rainfall Event over Chennai on 1 December 2015. *Mon. Weather Rev.* **2018**, *146*, 943–965. [CrossRef]
51. Seenirajan, M.; Natarajan, M.; Thangaraj, R.; Bagyaraj, M. Study and Analysis of Chennai Flood 2015 Using GIS and Multicriteria Technique. *J. Geogr. Inf. Syst.* **2017**, *09*, 126–140. [CrossRef]
52. Schicker, I.; Arnold, D.; Morton, D.; Seibert, P. Effects of updated land-use in WRF over mountainous terrain. *Am. Geophys. Union* **2011**, *2011*, A53B-0339.
53. Easton, M. How Much of Your Area is Built on? *BBC News*. 2017. Available online: https://www.bbc.com/news/uk-41901294 (accessed on 25 January 2022).
54. Hamdy, O.; Zhao, S.; Salheen, M.A.; Eid, Y.Y. Identifying the Risk Areas and Urban Growth by ArcGIS-Tools. *Geosciences* **2016**, *6*, 47. [CrossRef]
55. Esri. GIS Mapping Software, Location Intelligence & Spatial Analytics. 2021. Available online: https://www.esri.com/en-us/home (accessed on 18 August 2021).
56. Tropical Rainfall Measuring Mission (TRMM). *TRMM (TMPA) Rainfall Estimate L3 3-Hour 0.25-Degree x 0.25-Degree V7*; Goddard Earth Sciences Data and Information Services Center (GES DISC): Greenbelt, MD, USA, 2011. Available online: https://disc.gsfc.nasa.gov/datasets/TRMM_3B42_7/summary (accessed on 14 July 2020).
57. Subramanya, K. *Engineering Hydrology*, 5th ed.; McGraw-Hill: New Delhi, India, 2020.
58. Konrad, C. Effects of Urban Development on Floods. In U.S. Geological Survey Fact Sheet 076-03. 2016. Available online: https://pubs.usgs.gov/fs/fs07603/ (accessed on 17 August 2021).
59. Li, K.; Tian, F.; Khan, M.Y.A.; Xu, R.; He, Z.; Yang, L.; Lu, H.; Ma, Y. A High-Accuracy Rainfall Dataset by Merging Multiple Satellites and Dense Gauges over the Southern Tibetan Plateau for 2014–2019 Warm Seasons. *Earth Syst. Sci. Data* **2021**, *13*, 5455–5467. [CrossRef]
60. Rosenfeld, D.; Zheng, Y.; Hashimshoni, E.; Pöhlker, M.L.; Jefferson, A.; Pöhlker, C.; Yu, X.; Zhu, Y.; Liu, G.; Yue, Z.; et al. Satellite Retrieval of Cloud Condensation Nuclei Concentrations by Using Clouds as CCN Chambers. *PNAS* **2016**, *113*, 5828–5834. [CrossRef] [PubMed]